Journal of Biomechanics 44 (2011) 2482–2488

Contents lists available at ScienceDirect

Journal of Biomechanics

journal homepage: www.elsevier.com/locate/jbiomech
www.JBiomech.com

Tensile properties of rat femoral bone as functions of bone volume fraction, apparent density and volumetric bone mineral density

Ara Nazarian [a,*], Francisco J. Araiza Arroyo [a], Claudio Rosso [a,c], Shima Aran [a], Brian D. Snyder [a,b]

[a] Center for Advanced Orthopaedic Studies, Beth Israel Deaconess Medical Center and Harvard Medical School, Boston, MA, USA
[b] Department of Orthopaedic Surgery, Children's Hospital, Harvard Medical School, Boston, MA, USA
[c] Orthopaedic Department, University Hospital Basel, Basel, Switzerland

ARTICLE INFO

Article history:
Accepted 15 June 2011

Keywords:
Tensile properties
Osteomalacia
Ovariectomy
Rat
Bone
ρ_{APP}
BMC
Bone volume fraction
Bone mineral density
Apparent bone density

ABSTRACT

Mechanical testing has been regarded as the gold standard to investigate the effects of pathologies on the structure–function properties of the skeleton. Tensile properties of cancellous and cortical bone have been reported previously; however, no relationships describing these properties for rat bone as a function of volumetric bone mineral density (ρ_{MIN}), apparent density or bone volume fraction (BV/TV) have been reported in the literature.

We have shown that at macro level, compression and torsion properties of rat cortical and cancellous bone can be well described as a function of BV/TV, apparent density or ρ_{MIN} using non-destructive micro-computed tomographic imaging and mechanical testing to failure. Therefore, the aim of this study is to derive a relationship expressing the tensile properties of rat cortical bone as a function of BV/TV, apparent density or ρ_{MIN} over a range of normal and pathologic bones.

We used bones from normal, ovariectomized and osteomalacic animals. All specimens underwent micro-computed tomographic imaging to assess bone morphometric and densitometric indices and uniaxial tension to failure.

We obtained univariate relationships describing 74–77% of the tensile properties of rat cortical bone as a function of BV/TV, apparent density or ρ_{MIN} over a range of density and common skeletal pathologies. The relationships reported in this study can be used in the structural rigidity to provide a non-invasive method to assess the tensile behavior of bones affected by pathology and/or treatment options.

1. Introduction

Conventional mechanical testing has historically been regarded as the gold standard for investigating the effects of various interventions and pathologies on the structure–function properties of the skeleton (Danielsen et al., 1993; Turner and Burr, 1993). Recent advances in speed, resolution and reduction of artifacts in medical imaging (Genant et al., 2000) and the increasing computing power of personal computers (Moore, 1965) have made virtual alternatives to conventional and invasive procedures increasingly feasible (Bagi et al., 1992; Ferretti et al., 1995; van Rietbergen et al., 2002; Martin et al., 2004). The assessment of mechanical strength of skeletal tissue through alternative non-destructive means, virtual biomechanics, enable us to perform longitudinal in-vivo assessment of bone strength, facilitate the evaluation of multiple skeletal sites from the same subject, reduce the number of subjects and consequently the costs associated with a study. Additionally, the large experimental errors linked to operator dependent procedures such as specimen preparation and gripping (Odgaard and Linde, 1991; Keaveny et al., 1997) and inter-laboratory testing protocol differences can be reduced (Turner, 1989).

Both tissue material and geometric properties are considered in the analysis of bone strength. Currently, virtual biomechanics methods can be categorized into patient-specific finite element analysis (FEA) (Martin, 1991; Bessho et al., 2007), direct strength assessment such as dual-energy X-ray absorptiometry (DXA) (Kanis et al., 2000) or quantitative computed tomography (QCT) (Lochmuller et al., 2002; Buckley et al., 2007). Patient-specific FEA accounts for changes in the tissue material and geometric properties, but it is costly (Guldberg et al., 1998). Fracture predictions using DXA, as relatively crude 2D projection of 3D structures, are more cost-effective. However, it is neither sensitive nor specific, as it does not consider changes in material or geometric properties of bone (Riggs and Melton, 2002; Heaney, 2003; Schuit et al., 2004). QCT imaging (Faulkner et al., 1991; Lang et al., 1997; Lang

* Corresponding author. Tel.: 617 667 2940; fax: 617 667 7175.
E-mail address: anazaria@bidmc.harvard.edu (A. Nazarian).

0021-9290/$ - see front matter © 2011 Elsevier Ltd. All rights reserved.
doi:10.1016/j.jbiomech.2011.06.016

et al., 1998; Beck, 2003) is more accurate and provides information on both material and geometric properties of bone, but it is associated with significant radiation exposure.

We have introduced a method called Structural Rigidity Analysis (SRA) to supplement the currently available FE, DXA and QCT based methods to non-invasively assess the axial, bending and torsional properties of bones from their transaxial cross-sectional images (Hong et al., 2004). We have validated this technique using a series of ex-vivo (Whealan et al., 2000; Hong et al., 2004), in-vivo (Aaron et al., 2002; Snyder et al., 2006) and animal experiments (Entezari et al., 2011; Nazarian et al., 2010). With SRA, modulus of elasticity is treated as a function of bone density, and bone geometry is represented by its cross-sectional area and moment of inertia (Martin, 1991; Turner, 2002). We have previously reported the compressive (Cory et al., 2009) and torsional (Nazarian et al., 2009) properties of rat cancellous and cortical bones (cortical and cancellous bone for compression and cortical bone for torsion, from rat femora) as functions of bone volume fraction (BV/TV) or density. In order to extend the application of virtual biomechanics to the animal models, establishing the tensile properties of rat bone is an important step to conduct SRA on rat bones for any loading condition by validating empirical relationships that describe mechanical properties of any bone as a function of density.

We hypothesize that either bone mineral density (BMD), BV/TV or apparent density accounts for the majority of changes in the mechanical properties of Sprague Dawley rat bone at a macro-level. Therefore, our aim is to develop univariate relationships expressing axial tensile mechanical properties of whole rat bone as a function of μCT-based BMD, BV/TV or apparent density over a range of normal and pathologic bones.

2. Materials and methods

2.1. Animal model

The study protocol was approved by Beth Israel Deaconess Medical Center's Institutional Animal Care and Use Committee (IACUC). Thirty three female Sprague Dawley (SD, mass: 176–200 g – 12-weeks old) rats were obtained from Charles River Laboratories (Charles River, Charlestown, MA, USA) and were divided into three equally sized groups: control (CON), ovariectomy (OVX) and an osteomalacia (OM). The animals in the CON group were not subject to any surgical or dietary interventions; the animals in the OVX group underwent ovariectomy (a week prior to the start of the study) to induce a state of low bone mass and micro-architectural deterioration (Miller and Wronski, 1993; Guo and Goldstein, 2000; Ito et al., 2005; Kaczmarczyk-Sedlak et al., 2005; Ogawa et al., 2005); and the animals in the OM group were placed on an irradiated vitamin-D deficient diet (based on the 5755 purified standard rodent diet) containing 0.4% calcium and 0 vitamin-D_3 (from time zero till the end of the study) to induce osteomalacia (Anderson et al., 2008). Animals were weighed every 3-weeks to assess changes in the body mass. CON, OVX and OM animals were euthanized via CO_2 inhalation 12-weeks after arrival at the animal facility based on the previous studies assessing the onset of quantifiable manifestations of ovariectomy by our group (Nazarian et al., 2008a,b; Cory et al., 2009) and others (Katsuta et al., 1994; Oste et al., 2005).

2.2. Imaging and image analysis

Areal bone mineral density (ρ_{APP}, g cm^{-2}) and bone mineral content (BMC, g) at the distal femoral metaphysis (cancellous bone) and the femoral diaphysis (cortical bone) were measured using DXA (Lunar PIXImus2, General Electric, Waukesha, WI, USA) every 3-weeks. Two landmark-based analysis boxes, one to cover the cortical bone area and the other to cover the distal femoral metaphysis, were used to assess ρ_{APP} and BMC from DXA throughout the study.

At the end of the study, the animals were euthanized and both femurs were extracted. Sequential transaxial images through the entire cortical bone section were obtained using micro-computed tomography (μCT; μCT40, Scanco Medical, AG, Brüttisellen, Switzerland) at an isotropic voxel size of 30 μm, integration time of 250 ms, tube voltage and current of 55 keV and 145 μA, respectively, while applying a 1200 mg cm^{-3} hydroxyapatite (HA) beam hardening correction.

The images were binarized to separate bone from background using an established adaptive thresholding procedure (Kim et al., 2007). A three-dimensional Gaussian filter ($\sigma=0.8$) with a limited, finite filter support (support=1) was used to suppress the noise in the volumes. The optimum threshold was chosen automatically as a result of an iterative process, where successive iterations provided increasingly cleaner extractions of the object region.

After applying the adaptive thresholding algorithm, cortical (Ct.BV/TV) BV/TV and cortical thickness (Ct.Th) were assessed for all images (Hildebrand et al., 1999). Cortical ρ_{MIN} (ρ_{MIN}, g cm^{-3}) and apparent bone density (ρ_{APP}, g cm^{-3}) were also measured using a hydroxyapatite phantom, supplied by the manufacturer, to convert X-ray attenuation coefficient (μ) to mineral density. The variability of μCT assessment of 3D microstructural and densitometric indices of excised rat bone samples is less than 0.5% at our laboratory. The cross-sectional area of bone for each slice was calculated by counting the number of the bone voxels and multiplying by pixel size. Then, the cross-section with the minimum

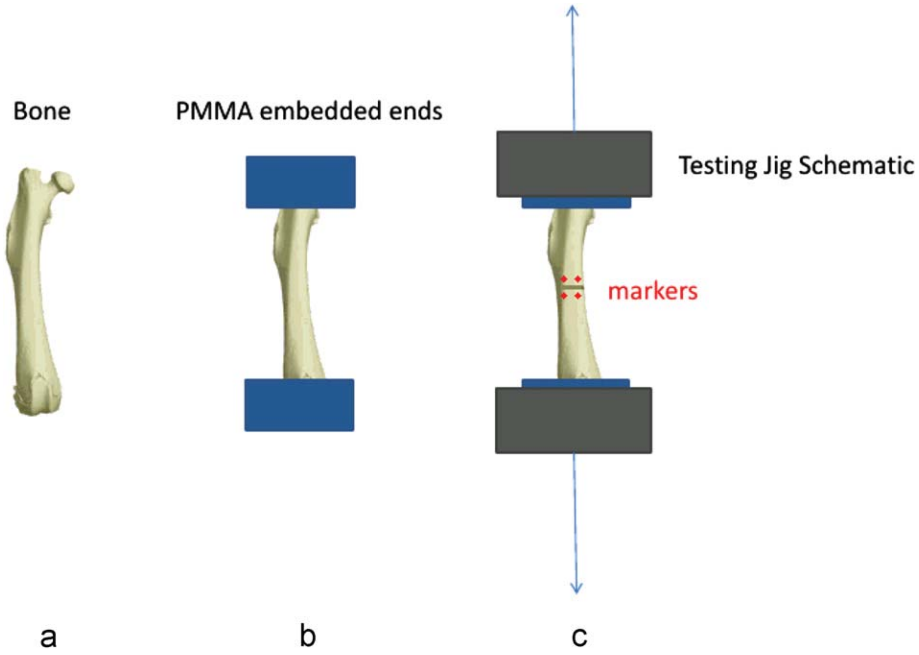

Fig. 1. (a) Illustration of the bone after removal of adherent soft tissue; (b) illustration of the bone after being embedded; (c) illustration of the bone with camera markers placed in the testing jig.

bony area was used to calculate the axial strength. The average cross-sectional area variation of cortical specimens was 18%.

2.3. Specimen preparation

After dissection and cleaning of all adherent soft tissues (Fig. 1a), poly methyl methacrylate (PMMA) was used to embed both ends of each femur for testing (Fig. 1b); Skripitz and Aspenberg, 1999). Once embedded, the femur was placed and held with rods inside two specially designed aluminum boxes in order to manipulate the sample without touching and causing the bone to fracture. Afterwards, the sample was placed in a custom-made apparatus and was held in position with aluminum plates on each side (Fig. 2). This apparatus was designed to shave a concentric stress riser notch (depth: 0.50 mm, width: 0.50 mm) along the surface of the bone and perpendicular to its long axis using a small diamond wafering blade on a low-speed saw (Isomet, Buehler Corporation, Lake Bluff, IL, USA) under copious irrigation.

The wafering blade was sandwiched between two plastic disks that were 0.5 mm smaller in radius than the blade to guarantee the desired stress riser depth. After indenting the bone, two Torlon rods, held by set screws, were positioned on each side of the two boxes holding the sample in a straight position during the imaging process to avoid premature overloading and fracture of the bone during handling (Fig. 2).

2.4. Mechanical testing

Specimens were thawed to room temperature 3 h before testing and hydrated prior to mechanical testing; otherwise, they were stored in 0.9% saline-soaked gauze at $-20\,^{\circ}C$. Markers were placed on each side of the stress riser notch to be used as reference points for the camera to assess mid-axis strain during biomechanical testing (Fig. 1c).

The aluminum boxes were placed on two custom designed holders (Fig. 3) to which adapters were attached and used to mount the load cell (Burster 8417 Subminiature Tension/Compression load cell, Gernsbach, Germany—range 1000 N, accuracy $< \pm 0.5\%$ full scale output). When under tension, the load cell was in line with the stainless steel cables holding the bone in position (Fig. 3). Once the starting position was reached, the Torlon bars were removed to allow the bone to undergo uniaxial tension to failure at a strain rate of $0.005\ s^{-1}$ (Synergy 200, MTS Systems, Eden Prairie, MN, USA) (Fig. 4).

A high speed camera (PixeLINK CMOS microscopy camera model PL-B681C, Ottawa, ON, Canada) captured images at a rate of 20 frames/s throughout testing after having passed a calibration procedure with a calibration glass. A Matlab (MATLAB v12.0, Mathworks, Natick, MA, USA) program was used to assess mid-axis strain by measuring the differences in distances between the centroids of the markers in each image (placed above and below the stress riser notch).

Stiffness (K, $kN\,mm^{-1}$), ultimate displacement (d_{ULT}, mm) and ultimate load (L_{ULT}, kN) representing intrinsic structural properties, were measured for the study. Additionally, extrinsic properties such as tensile modulus (E, MPa), ultimate strain (ε_{ULT}, mm/mm), ultimate strength (σ_{ULT}, MPa) and energy to failure (Energy, J) were calculated for all specimens.

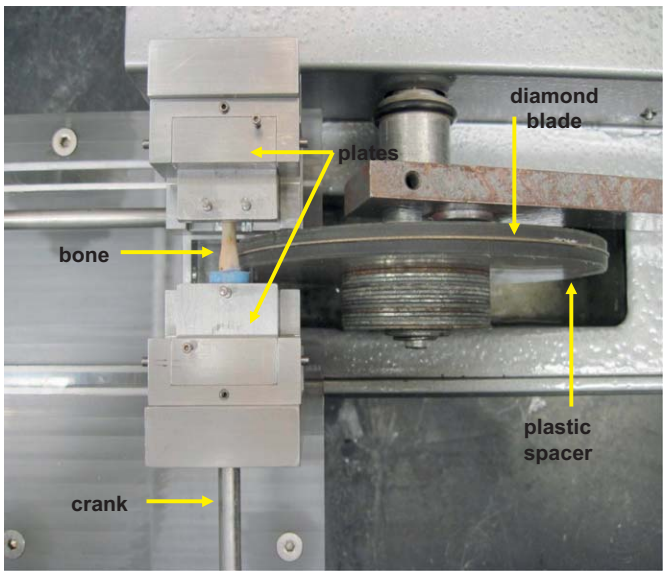

Fig. 2. Image of the shaving device and the cutting machine completely assembled and positioned before the start of the process.

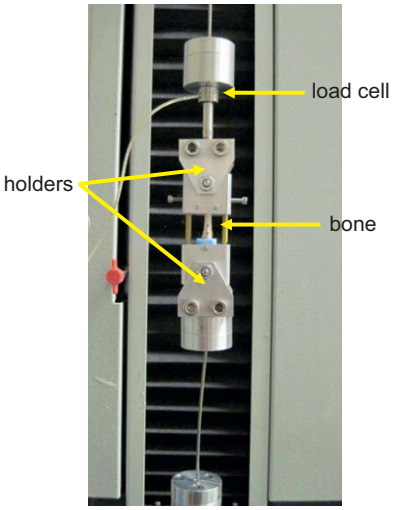

Fig. 3. Image of a bone specimen positioned on the tensile testing system prior to testing.

2.5. Statistical analysis

Continuous data were assessed for normality using the Kolmogorov–Smirnov test. Univariate regression analysis was conducted to examine whether the modulus of elasticity of cortical SD rat bone could be expressed as a function of BV/TV, apparent density, or ρ_{MIN} (all obtained from μCT imaging). To assess whether the densitometric, structural and mechanical properties measured for this study were different for the CON, OVX and OM groups, a one-way Analysis of Variance (ANOVA) with a Bonferroni correction for multiple comparisons was conducted with groups as fixed factor and force (N), BV/TV (BV/TV, $mm^3\,mm^{-3}$), apparent bone density (ρ_{APP}, $mg\,HA\,cm^{-3}$) ρ_{MIN} (ρ_{MIN}, $mg\,HA\,cm^{-3}$), DXA based ρ_{APP}, ($g\,cm^{-2}$) and bone mineral content (BMC, g), ultimate load (L_{ULT}, N), ultimate displacement (d_{ULT}, mm), stiffness (K, $N\,mm^{-1}$), ultimate stress (σ_{ULT}, MPa), ultimate strain (ε_{ULT}, $mm\,mm^{-1}$), modulus of elasticity (E, MPa) and energy to failure (Energy, J) as dependent parameters.

The SPSS software (version 17.0, Chicago, IL, USA) was used for data analysis. All reported p-values are two-tailed with $p < 0.05$ considered statistically significant.

3. Results

Univariate regression analysis revealed that the modulus of elasticity and tensile yield strength can be expressed as a linear function of BV/TV, apparent bone density and ρ_{MIN} (Table 1 and Fig. 4).

Analysis of variance revealed significant inter-group differences in the densitometric, structural and mechanical properties of the bones measured in this study. There were significant differences in BV/TV, μCT based apparent and mineral densities and mechanical testing based ultimate displacement and load, ultimate strain and stress and modulus of elasticity ($P < 0.01$ for all cases). No significant differences in DXA-based ρ_{APP} ($p = 0.159$), BMC ($p = 0.133$), mechanical testing based stiffness ($p = 0.321$) and energy to failure ($p = 0.14$) were observed when comparing the data between the CON, OVX and OM groups. DXA based ρ_{APP} and BMC failed to register any differences between the three groups in post-hoc analysis ($p > 0.159$ for all cases).

BV/TV and apparent density in the control group were higher than those of the OVX and OM groups ($p < 0.03$ for BV/TV and apparent density). The BV/TV between the OVX and OM groups were not different from one another ($p = 0.284$ and 0.165, respectively). BMD in the control group was higher than that of the OM group, which was in turn higher than that of the OVX group ($p < 0.04$ for all cases). Ultimate stress in the CON group was greater than those of the OVX and OM groups ($p < 0.005$ for all cases), yet no difference in ultimate stress was observed between the OVX and OM groups ($p = 0.99$).

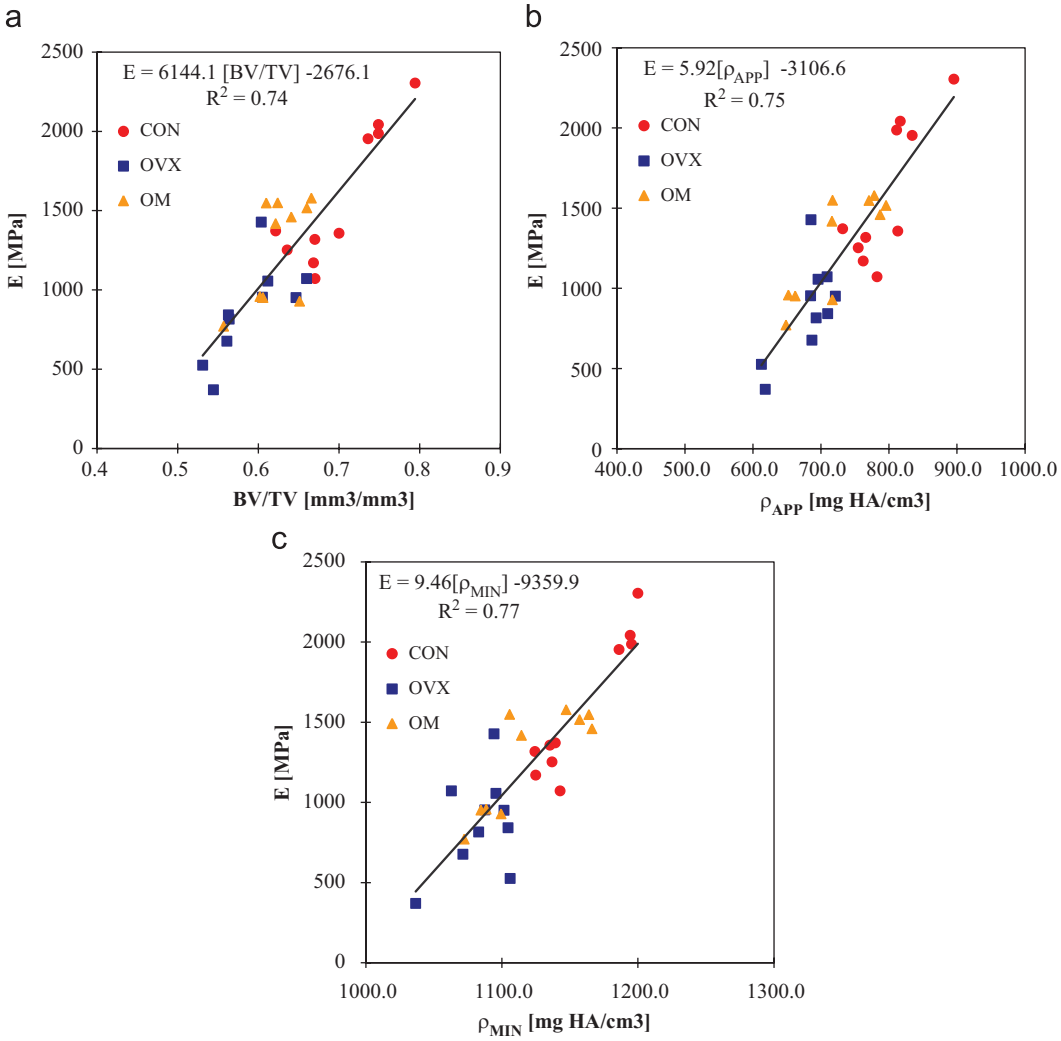

Fig. 4. Univariate relationships describing the behavior of the modulus of elasticity based on the independent variable of volumetric bone mineral density (a), apparent density (b) and bone volume fraction (c).

Table 1
A univariate linear relationship of the variation in modulus of elasticity and yield strength with BV/TV, ρ_{APP} or ρ_{MIN} as the independent variable.

	Modulus of elasticity			Tensile yield strength	
	E	R^2	Fig.	σ_Y	R^2
Bone volume fraction (BV/TV)	6144.1(BV/TV) − 2676.1	0.74	4a	145.4[BV/TV] − 9.9	0.71
Apparent bone density (ρ_{APP})	5.92ρ_{APP} − 3106.6	0.75	4b	0.04ρ_{APP} − 13.02	0.72
Volumetric BMD (ρ_{MIN})	9.46ρ_{MIN} − 9359.9	0.77	4c	0.06ρ_{MIN} − 51.17	0.69

4. Discussion

The incorporation of pathologic bones from ovariectomized and vitamin-D deficient animals enhances the range of bone density and provides a relationship that describes both normal and pathologic bones. In all the cases, cortical bone of the OVX group occupies the nearest position to the lower left quadrant of each graph corresponding to the lowest density/strength and volume/strength relations. Cortical bone of the OM group overlaps with the highest and lowest values of the OVX and CON groups, respectively. Meanwhile, cortical bone of the control group occupies the top right quadrant of each graph corresponding to the highest density/strength and volume/strength relations (Table 2).

The univariate strength equation with mineral density as the descriptor variable provides a convenient means to convert density to strength, which will be useful in studies where the effects of a pathologic condition and/or a pharmacologic agent on the bone strength are examined using the now laboratory standard μCT imaging systems. Likewise, the strength equation based on apparent density provides a conversion means for studies not based on μCT imaging. The strength equation based on BV/TV provides a means where strength of bone can be described by the amount of bone present. Such an equation is useful in cases where a pathologic condition or a pharmacologic agent specifically alters the amount of bone. The three relationships of this study are derived from the same animals using the same methods, allowing for cross conversion and interpretation

Table 2
Densitometric and mechanical properties of cortical bones from three models (CON, OVX and OM). The parameters reported in the table are: BV/TV: bone volume fraction, Ct.Th: cortical thickness, ρ_{APP}: apparent bone density, ρ_{MIN}: volumetric bone mineral density, ρ_{APP}: areal bone mineral density, BMC: bone mineral content, L_{ULT}: ultimate load, d_{ULT}: ultimate displacement, K: stiffness, σ_{ULT}: ultimate stress, ε_{ULT}: ultimate strain, E: modulus of elasticity and Energy: energy to failure.

		μCT				DXA		Mechanical testing						
		BV/TV [mm^3/mm^{-3}]	Ct.Th [mm]	ρ_{APP} [$g\,cm^{-3}$]	ρ_{MIN} [$g\,cm^{-3}$]	ρ_{APP} [$g\,cm^{-2}$]	BMC [g]	L_{ULT} [N]	d_{ULT} [mm]	K [$N\,mm^{-1}$]	σ_{ULT} [MPa]	ε_{ULT} [$mm\,mm^{-1}$]	E [MPa]	Energy [J]
CON	**Mean**	0.699	0.612	796.67	1157.90	0.189	0.149	127.38	0.53	211.24	24.35	0.02	1583.14	1.19E-04
	Std. Dev.	0.056	0.032	47.48	31.71	0.018	0.011	32.97	0.20	86.59	6.09	0.01	439.44	8.12E-05
OVX	**Mean**	0.589	0.649	681.59	1084.32	0.191	0.159	108.76	0.74	164.10	15.82	0.02	869.38	1.22E-04
	Std. Dev.	0.043	0.039	36.97	21.90	0.020	0.014	41.18	0.30	56.10	5.85	0.01	300.14	7.81E-05
OM	**Mean**	0.624	0.613	724.49	1119.96	0.204	0.152	72.65	0.43	179.77	14.40	0.01	1268.63	6.67E-05
	Std. Dev.	0.033	0.036	56.87	35.57	0.015	0.006	26.44	0.10	62.89	4.39	0.00	322.10	3.14E-05
	P (ANOVA)	0.000	0.047	0.000	0.000	0.159	0.133	0.004	0.011	0.321	0.001	0.011	0.001	0.140
Bonferroni	P:CON–OP	0.000	0.088	0.000	0.000	0.990	0.159	0.699	0.114	0.427	0.005	0.114	0.000	0.990
	P:CON–OM	0.002	0.990	0.007	0.028	0.239	0.990	0.004	0.920	0.966	0.001	0.920	0.182	0.286
	P:OP–OM	0.284	0.103	0.165	0.042	0.336	0.467	0.076	0.010	0.990	0.990	0.010	0.058	0.236

of data, in cases where only one independent variable is available. Further improvement on the predictive powers of these regressions could be achieved by introducing morphometric indices that can better account for the variations in bone 3D microstructure. This can also reduce the variation in mechanical properties for any given density value.

Beaupied et al. (2006) have reported the mechanical properties of 12-week old Wistar rat femurs undergoing tensile testing to failure at a rate of 0.5 mm mm^{-1}. The modulus of elasticity values reported in this study (134.04–147.36 MPa) were on average an order of magnitude smaller than the values reported in the current study. The difference in the values could be due to variations in the testing methodologies, and the method in which the cross-sectional area was calculated in the Beaupied et al. study.

Comelekoglu et al. (2007) reported the densitometric and tensile properties of 4-month old female normal and ovariectomized Sprague Dawley rats. They reported femoral ρ_{APP} and cortical thickness values of 0.132–0.114 g cm^{-2} and 0.418–0.33 mm for the normal and OVX animals, respectively, which were lower than our results. They reported similar stiffness values for the normal bones (191.60 N mm^{-1}), and significantly lower values for the OVX animals (53.95 N mm^{-1}). They also reported similar ultimate stress values (23.71–18.91 MPa) to those reported in this study. However, the modulus of elasticity values reported in that study (79.43–37.92 MPa) are significantly lower than those reported here or expected from bone regions that were predominantly comprised of cortical bones. Errors in calculation of the modulus could explain the discrepancy in their results.

The empirical relationships reported in this study should be interpreted within the limitations associated with this type of study. In order to optimize the utility of an empirical relationship, one should improve the quality of the input sources, which in case of this study are mechanical testing and μCT imaging.

Uniaxial tension was selected as a mode of mechanical testing representing a portion of in-vivo loads applied to the skeleton, especially in bending scenarios, where one side of the bone is under tensile loading. The sources of error in mechanical testing could be variations in cross-sectional area or imaging and analysis methods. Although there are some limitations in quantitative measurement of bone density with any imaging modality, the current generation of μCT imaging systems errors in measured density and microstructural data are of the order of 0.5% based on the quality control measurements performed in our laboratory (Nazarian et al., 2008a,b).

The univariate relationships based on μCT (ionizing source) generated data can only assess the contribution of the mineral component of the bone to its overall strength, while ignoring the contribution of the matrix. Recent advances in solid state Magnetic Resonance (MR) imaging have enabled the quantitative assessment of mineral and matrix components of bone using a non-ionizing imaging modality (Cao et al., 2009). As the resolution gap between these two modalities is narrowing, it is increasingly possible to establish relationships that account for changes in both mineral and matrix components of bone non-invasively in the near future.

Previously, a power law relationship was used to describe the compressive properties of rat trabecular and cortical bone as a function of BV/TV, apparent or mineral density (Cory et al., 2009). However, it could not be employed to describe the tensile properties, since we only had specimens from regions that were comprised of cortical bone specimens in this study. Accordingly, the volume fraction or density range for the bones was not large enough to allow for power law data fitting. The authors originally aimed to include both cortical and trabecular bone specimens in the study and planned to use the notching technique to shave off the cortical bone in the distal metaphyseal bone area thereby exposing a trabecular bone, the only region to be subjected to tension. However, the proximity of the notch to the distal end of the bone and the PMMA embedding precluded the possibility of accurate mechanical testing.

There are a number of approaches in virtual biomechanics to determine bone strength from imaging parameters (Faulkner et al., 1991; Lang et al., 1997; Lang et al., 1998; Riggs and Melton, 2002; Beck, 2003; Heaney, 2003; Schuit et al., 2004). The SRA, which is

predicated upon the use of empirical relationships to calculate rigidity of each cross-sectional image from the modulus-weighted area of each pixel, is one of them. The relationships generated from this study can be used to assess rigidity of rat bones as affected by different biologic or pharmaceutical agents. Other approaches are based on the creation of patient-specific models from 3D-images such as QCT and MRI to predict bone mechanical behavior via FE analysis. The correlations reported in this study can be employed in FE models to assign tissue properties to the models and incorporate the effects of density into the existing structure based FE models.

Conclusively, we have introduced univariate relationships to describe the tensile properties of rat bone based on BV/TV, BMD, or apparent density, which can describe the mechanical properties of rat cortical bone over a range of density and common skeletal pathologies. It is worthwhile to mention that virtual biomechanics is not aimed to replace conventional mechanical testing, as many mechanical properties simply cannot be quantified via virtual biomechanics, such as displacement and absorbed energy. However, virtual biomechanics can provide a first order simplified approach to assess the effects of pathology and/or pharmacologic agents on bone strength in a large throughput and cost-effective manner.

Conflict of interest statement

None declared.

Acknowledgements

The authors would like to acknowledge the Children's Hospital Orthopedic Surgery Foundation (B.D.S.) and the Swiss National Science Foundation SNF and the Swiss Society for Orthopedics and Traumatology (C.R.) for providing financial support for this project. Additionally, they would like to acknowledge Robert Fazio and Heitor Murato from the Boston University Scientific Instrument Facility for manufacturing the specimen preparation device.

References

Aaron, M., Snyder, B.D., Wilson, S., Kwak, D., Zurakowski, D., Coughlin, L., Parker, L., 2002. Noninvasive prediction of fracture risk in patients with metastatic breast cancer to the spine. In: Proceedings of the 47th Annual Meeting of the Orthopedic Research Society, Dallas, TX.

Anderson, P.H., Sawyer, R.K., et al., 2008. Vitamin D depletion induces RANKL-mediated osteoclastogenesis and bone loss in a rodent model. J. Bone Miner. Res., 23.

Bagi, C.M., Miller, S.C., et al., 1992. Differences in cortical bone in overloaded and underloaded femurs from ovariectomized rats: comparison of bone morphometry with torsional testing. Bone 13 (1), 35–40.

Beaupied, H., Dupuis, A., et al., 2006. The mode of bone conservation does not affect the architecture and the tensile properties of rat femurs. Biomed. Mater. Eng. 16 (4), 253–259.

Beck, T., 2003. Measuring the structural strength of bones with dual-energy X-ray absorptiometry: principles, technical limitations, and future possibilities. Osteoporosis Int. 14 (Suppl. 5), 81–88.

Bessho, M., Ohnishi, I., et al., 2007. Prediction of strength and strain of the proximal femur by a CT-based finite element method. J. Biomech. 40 (8), 1745–1753.

Buckley, J.M., Loo, K., et al., 2007. Comparison of quantitative computed tomography-based measures in predicting vertebral compressive strength. Bone 40 (3), 767–774.

Cao, H., Nazarian, A., et al., 2009. Quantitative ^{31}P NMR spectroscopy and ^{1}H MRI measurements of bone mineral and matrix density differentiate metabolic bone diseases in rat models. Bone 46 (6), 1582–1590 (Epub 2010 Feb 24).

Comelekoglu, U., Bagis, S., et al., 2007. Biomechanical evaluation in osteoporosis: ovariectomized rat model. Clin. Rheumatol. 26 (3), 380–384.

Cory, E., Nazarian, A., et al., 2009. Compressive axial mechanical properties of rat bone as functions of bone volume fraction, apparent density and micro-CT based mineral density. J. Biomech. 43 (5), 953–960.

Danielsen, C.C., Mosekilde, L., et al., 1993. Cortical bone mass, composition, and mechanical properties in female rats in relation to age, long-term ovariectomy, and estrogen substitution. Calcif. Tissue Int. 52 (1), 26–33.

Entezari, V., Basto, P.A., et al., 2011. Non–invasive assessment of failure torque in rat bones with simulated lytic lesions using computed tomography based structural rigidity analysis. J. Biomech 44 (3), 552–556 PMID: 20926079.

Faulkner, K.G., Glüer, C., et al., 1991. Noninvasive measurements of bone mass, structure, and strength: current methods and experimental techniques. Am. J. Radiol. 157, 1229–1237.

Ferretti, J.L., Gaffuri, O., et al., 1995. Dexamethasone effects on mechanical, geometric and densitometric properties of rat femur diaphyses as described by peripheral quantitative computerized tomography and bending tests. Bone 16 (1), 119–124.

Genant, H.K., Gordon, C., et al., 2000. Advanced imaging of the macrostructure and microstructure of bone. Horm. Res. 54 (Suppl. 1), 24–30.

Guldberg, R.E., Hollister, S.J., et al., 1998. The accuracy of digital image-based finite element models. J. Biomech. Eng. 120 (2), 289–295.

Guo, X.E., Goldstein, S.A., 2000. Vertebral trabecular bone microscopic tissue elastic modulus and hardness do not change in ovariectomized rats. J. Orthop. Res. 18 (2), 333–336.

Heaney, R.P., 2003. Is the paradigm shifting? Bone 33 (4), 457–465.

Hildebrand, T., Laib, A., et al., 1999. Direct three-dimensional morphometric analysis of human cancellous bone: microstructural data from spine, femur, iliac crest, and calcaneus. J. Bone Miner. Res. 14 (7), 1167–1174.

Hong, J., Cabe, G.D., et al., 2004. Failure of trabecular bone with simulated lytic defects can be predicted non-invasively by structural analysis. J. Orthop. Res. 22 (3), 479–486.

Ito, M., Nishida, A., et al., 2005. Effects of risedronate on trabecular microstructure and biomechanical properties in ovariectomized rat tibia. Osteoporosis Int. 16 (9), 1042–1048.

Kaczmarczyk-Sedlak, I., Janiec, W., et al., 2005. Effect of administration of etidronate and trtinol on bone mechanical properties in ovariectomized rats. Pharmacol. Rep. 57, 203–211.

Kanis, J.A., Johnell, O., et al., 2000. Prediction of fracture from low bone mineral density measurements overestimates risk. Bone 26 (4), 387–391.

Katsuta, O., Hiratsuka, H., et al., 1994. Cadmium-induced osteomalacic and osteopetrotic lesions in ovariectomized rats. Toxicol. Appl. Pharmacol. 126 (1), 58–68.

Keaveny, T.M., Pinilla, T.P., et al., 1997. Systematic and random errors in compression testing of trabecular bone. J. Orthop. Res. 15 (1), 101–110.

Kim, C.H., Zhang, H., et al., 2007. Effects of thresholding techniques on μCT-based finite element models of trabecular bone. J. Biomech. Eng. 129, 481–486.

Lang, T., Augat, P., et al., 1998. Noninvasive assessment of bone density and structure using computed tomography and magnetic resonance. Bone 22 (Suppl. 5), 149S–153S.

Lang, T.F., Keyak, J.H., et al., 1997. Volumetric quantitative computed tomography of the proximal femur: precision and relation to bone strength. Bone 21 (1), 101–108.

Lochmuller, E.M., Groll, O., et al., 2002. Mechanical strength of the proximal femur as predicted from geometric and densitometric bone properties at the lower limb versus the distal radius. Bone 30 (1), 207–216.

Martin, D.E., Severns, A.E., et al., 2004. Determination of mechanical stiffness of bone by pQCT measurements: correlation with non-destructive mechanical four-point bending test data. J. Biomech. 37 (8), 1289–1293.

Martin, R.B., 1991. Determinants of the mechanical properties of bones. J. Biomech. 24 (Suppl. 1), 79–88.

Miller, S.C., Wronski, T.J., 1993. Long-term osteopenic changes in cancellous bone structure in ovariectomized rats. Anat. Rec. 236 (3), 433–441.

Moore, G.E., 1965. Cramming more components onto integrated circuits. Electronics 38, 8.

Nazarian, A., Entezari, V., et al., 2009. An improved method to assess torsional properties of rodent long bones. J. Biomech. 42 (11), 1720–1725.

Nazarian, A., Pezzella, L., et al., 2010. Application of structural rigidity analysis to assess fidelity of healed fractures in rat femurs with critical defects. Calcif. Tissue Int. 86 (5), 397–403.

Nazarian, A., Snyder, B.D., et al., 2008a. Quantitative micro-computed tomography: a non-invasive method to assess equivalent bone mineral density. Bone 43, 302–311.

Nazarian, A., von Stechow, D., et al., 2008b. Bone volume fraction explains the variation in strength and stiffness of cancellous bone affected by metastatic cancer and osteoporosis. Calcif. Tissue Int.

Odgaard, A., Linde, F., 1991. The underestimation of Young's modulus in compressive testing of cancellous bone specimens. J. Biomech. 24 (8), 691–698.

Ogawa, K., Hori, M., et al., 2005. Effects of combined elcatonin and alendronate treatment on the architecture and strength of bone in ovariectomized rats. J. Bone Miner. Metab. 23 (5), 351–358.

Oste, L., Bervoets, A.R., et al., 2005. Time-evolution and reversibility of strontium-induced osteomalacia in chronic renal failure rats. Kidney Int. 67 (3), 920–930.

Riggs, B.L., Melton III, L.J., 2002. Bone turnover matters: the raloxifene treatment paradox of dramatic decreases in vertebral fractures without commensurate increases in bone density. J. Bone Miner. Res. 17 (1), 11–14.

Schuit, S.C., van der Klift, M., et al., 2004. Fracture incidence and association with bone mineral density in elderly men and women: the Rotterdam Study. Bone 34 (1), 195–202.

Skripitz, R., Aspenberg, P., 1999. Attachment of PMMA cement to bone: force measurements in rats. Biomaterials 20 (4), 351–356.

Snyder, B.D., Hauser-Kara, D.A., et al., 2006. Predicting fracture through benign skeletal lesions with quantitative computed tomography. J. Bone Jt. Surg. Am. 88 (1), 55–70.

Turner, C., 1989. Yield behavior of bovine cancellous bone. J. Biomech. Eng. 111, 256–260.

Turner, C.H., 2002. Determinants of skeletal fragility and bone quality. J. Musculoskelet. Neuronal Interact. 2 (6), 527–528.
Turner, C.H., Burr, D.B., 1993. Basic biomechanical measurements of bone: a tutorial. Bone 14 (4), 595–608.
van Rietbergen, B., Majumdar, S., et al., 2002. High-resolution MRI and micro-FE for the evaluation of changes in bone mechanical properties during longitudinal clinical trials: application to calcaneal bone in postmenopausal women after one year of idoxifene treatment. Clin. Biomech. (Bristol, Avon) 17 (2), 81–88.
Whealan, K.M., Kwak, S.D., et al., 2000. Noninvasive imaging predicts failure load of the spine with simulated osteolytic defects. J. Bone Jt. Surg. Am. 82 (9), 1240–1251.